Celest Mech Dyn Astr (2015) 121:329–346
DOI 10.1007/s10569-015-9605-8

ORIGINAL ARTICLE

Earth–Mars transfers with ballistic capture

F. Topputo · E. Belbruno

Received: 10 November 2014 / Revised: 25 January 2015 / Accepted: 28 January 2015 /
Published online: 10 February 2015

Abstract We construct a new type of transfer from the Earth to Mars, which ends in ballistic capture. This results in substantial savings in capture Δv from that of a classical Hohmann transfer under certain assumptions as well as an alternate way for spacecraft to transfer to Mars. This is accomplished by first becoming captured at Mars, very distant from the planet, and then from there, following a ballistic capture transfer to a desired altitude within a ballistic capture set. This is achieved by using stable sets, which are sets of initial conditions whose orbits satisfy a definition of orbital stability. This transfer type may be of interest for Mars missions because of low capture Δv, flexibility of launch period from the Earth, moderate flight time, and the benign nature of the capture process.

Keywords Ballistic capture · Restricted three-body problem · Mars transfer · Low energy transfers · Weak stability boundary

1 Introduction

In 1991 the Hiten spacecraft of Japan used a new type of transfer to the Moon, using ballistic capture (Belbruno and Miller 1993). This is a capture where the Kepler energy of the spacecraft with respect to the Moon becomes negative from initially positive values, by only using the natural gravitational forces of the Earth, Moon, and Sun. It is generally temporary (Topputo et al. 2008; Belbruno et al. 2008). This capture uses substantially less Δv than a Hohmann transfer which has a positive v_∞ at lunar approach, making it an attractive alter-

F. Topputo (✉)
Department of Aerospace Science and Technology, Politecnico di Milano, Via La Masa, 34, 20156 Milan, Italy
e-mail: francesco.topputo@polimi.it

E. Belbruno
Department of Astrophysical Sciences, Princeton University, Peyton Hall, Ivy Lane, Princeton, NJ 08544, USA
e-mail: belbruno@princeton.edu

native for lunar missions. This same type of transfer was, in fact, used by NASA's GRAIL mission in 2011 (Chung et al. 2010). Another type of ballistic capture transfer first found in 1986 (Belbruno 2004), was used in 2004 by ESA's SMART-1 mission (Schoenmaekers et al. 2001).

Since ballistic capture occurs about the Moon in a region called a weak stability boundary, these transfers are called weak stability boundary transfers or ballistic capture transfers. The types that were used for Hiten and GRAIL are called *exterior* transfers since they first go beyond the orbit of the Moon. The types used for SMART-1 are called *interior* transfers since they remain within the Earth–Moon distance (Belbruno 2004). They are also referred to as low energy transfers, since they use less Δv for capture (Topputo 2013). The weak stability boundary, in general, has recently been shown to be a complex Cantor-like region consisting of a network of invariant manifolds, associated to the collinear Lagrange points, L_1, L_2 (Belbruno et al. 2010, 2013). The dynamics of motion in this region is chaotic and unstable, thus explaining why the capture is temporary.

Ever since these ballistic capture transfers to the Moon were discovered, it was natural to ask if there were transfers from the Earth that led to ballistic capture at Mars. It was generally felt that Hiten-like transfers did not exist after a number of efforts (Lo and Ross 1998; Castillo et al. 2003; Topputo et al. 2005; Mingotti et al. 2011). The reason for this is that the orbital velocity of Mars is much higher than the approach v_∞ of a Hohmann transfer from the Earth, whereas the v_∞ of a Hohmann transfer to the Moon is close to the Moon's orbital velocity.

The purpose of this paper is to show that ballistic capture transfers to Mars, from the Earth, do exist. We will show how to construct them. The key idea is not to try to find transfers from the Earth that go directly to ballistic capture near to Mars. But rather, to first transfer to ballistic capture far from Mars, several millions of kilometers away from Mars, yet close to its orbit about the Sun. At first it would seem counter intuitive to first transfer so far from Mars. At this distant location, ballistic capture transfers can be found that go close to Mars after several months travel time, in the examples given, and then into ballistic capture. This results in elliptic-type orbits about Mars. We show in the examples presented that for capture periapsis altitudes higher than 22,000 km, these transfers from the Earth use considerably less Δv than a Hohmann transfer under the given assumptions. At altitudes less than this, it is found that the Hohmann transfer uses only slightly less capture Δv, which may make the ballistic capture alternative presented here more desirable. This is because by transferring from the Earth to points far from Mars near Mars orbit, it is not necessary to adhere to a two-year launch period from the Earth. The times of launch from the Earth can be much more flexible. Thus, it is not just the capture Δv that is of interest, but also the consideration of the more flexible launch period. Moreover, the use of this new transfer has several other advantages for Mars missions. This includes a benign capture process with relatively little risk. The initial capture locations along Mars orbit may be of interest for operational purposes.

The structure of this paper is as follows: In Sect. 2, we describe the methodology and steps that we will use to find these new transfers. In the remaining sections, these steps are elaborated upon. In Sect. 3, we describe the basic model used to compute the trajectories, planar elliptic restricted three-body problem. In Sect. 4, the stable sets at Mars are described, whose manipulation allows us to achieve the capture sets. In Sect. 5 we describe interplanetary transfers from Earth to locations far from Mars that are at the beginning of ballistic capture transfers to Mars. In Sect. 6 comparisons to Hohmann transfers are made. In Sect. 7 applications are discussed and future work. Two appendixes are reported where complementary material is presented.

2 Methodology and steps

The new class of ballistic capture transfers from Earth to Mars are constructed in a number of steps. These steps are as follows:

Step 1 Compute a ballistic capture trajectory (transfer) to Mars to a given periapsis distance, r_p. The trajectory starts far from Mars at a point $\mathbf{x}_c$, near Mars orbit. In this paper $\mathbf{x}_c$ is chosen several million kilometers from Mars. $\mathbf{x}_c$ corresponds to the start of a trajectory that goes to ballistic capture near Mars, after a maneuver, ΔV_c, is applied (defined in the next step). Although this location is far from Mars, we refer to it as a capture maneuver, since the trajectory eventually leads to ballistic capture. It takes, in general, several months to travel from $\mathbf{x}_c$ to ballistic capture near Mars to the periapsis distance, r_p. When the spacecraft, P, arrives at the distance r_p, its osculating eccentricity, e, with respect to Mars is less than 1. Once the trajectory moves beyond the capture at the distance r_p, it is in a special capture set where it will perform a given number of orbits about Mars. The simulations in this step use the planar elliptic restricted three-body problem (see Fig. 1).

Step 2 An interplanetary transfer trajectory for P starts at the sphere of influence (SOI) of the Earth. A first maneuver, ΔV_1, is applied to transfer to the point $\mathbf{x}_c$ near Mars orbit, where a second maneuver, ΔV_c, is used to match the velocity of the ballistic capture transfer to Mars. This transfer from Earth is in heliocentric space and is viewed as a two-body problem between P and the Sun. The maneuver ΔV_c is minimized using an optimization algorithm, which adjusts the location of $\mathbf{x}_c$.

Step 3 The trajectory consisting of the interplanetary transfer to $\mathbf{x}_c$ together with the ballistic capture transfer from $\mathbf{x}_c$ to the distance r_p from Mars, where the osculating eccentricity $e < 1$, is the resulting ballistic capture transfer from the Earth. This is compared to a standard Hohmann transfer leaving the Earth from the SOI and going directly to the distance r_p from Mars with the same eccentricity e, where a ΔV_2 is applied at the distance r_p to achieve this eccentricity. ΔV_2 is compared to ΔV_c. It is found in the cases studied, that for $r_p > 22,000$ km, we can achieve $\Delta V_c < \Delta V_2$. For example, it is shown that if r_p is about 92, 000km, then ΔV_c is about 15 % less then ΔV_2. It is shown that by transferring to much lower altitudes from these r_p values yields only a relatively small increase from the capture Δv required for a Hohmann transfer. As is explained in latter sections, this may make the ballistic capture transfer more desirable in certain situations.

The main reasons $\mathbf{x}_c$ is chosen far from Mars is three-fold. First, if $\mathbf{x}_c$ is sufficiently far from the Mars SOI, there is a negligible gravitational attraction of Mars on P. This yields a more constant arrival velocity from the Earth in general. Second, since the points, $\mathbf{x}_c$, lie near to Mars orbit, there are infinitely many of them which offer many locations to start a ballistic capture transfer. This variability of locations gives flexibility of the launch period from the Earth. Third, since $\mathbf{x}_c$ is outside the SOI of Mars, the application of ΔV_c can be done in a gradual manner, and from that point on, no more maneuvers are required, where P arrives at the periapsis distance r_p in a natural capture state. This process is much more benign than the high velocity capture maneuver at r_p typical of an Hohmann transfer, which is subject to single-point failures. From an operational point of view, this is safer.

We now describe these steps in detail in the following sections.

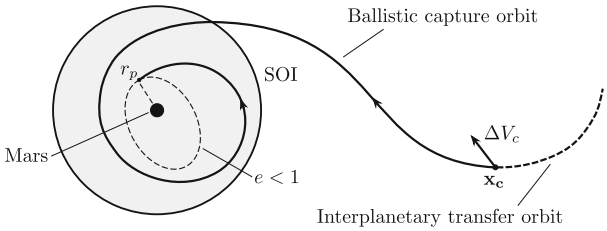

Fig. 1 Structure of the ballistic capture transfers to Mars

3 Model

When our spacecraft, P, is in motion about Mars, from arrival at $\mathbf{x}_c$ to Mars ballistic capture at r_p, we model the motion of P by the planar elliptic restricted three-body problem, which takes into account Mars eccentricity, $e_p = 0.093419$. Because the mass of P is negligible with respect to that of the Earth or Mars, it can be chosen to be zero.

The planar elliptic restricted three-body problem studies the motion of a massless particle, P, under the gravitational field generated by the mutual elliptic motion of two primaries, P_1, P_2, of masses m_1, m_2, respectively. In this paper, P_1 is the Sun and P_2 is Mars. The equations for the motion of P are

$$x'' - 2y' = \omega_x, \qquad y'' + 2x' = \omega_y. \tag{1}$$

The subscripts in Eq. (1) are the partial derivatives of

$$\omega(x, y, f) = \frac{\Omega(x, y)}{1 + e_p \cos f}, \tag{2}$$

where the potential function is

$$\Omega(x, y) = \frac{1}{2}\left(x^2 + y^2\right) + \frac{1-\mu}{r_1} + \frac{\mu}{r_2} + \frac{1}{2}\mu(1-\mu), \tag{3}$$

and $r_1 = \left[(x+\mu)^2 + y^2\right]^{1/2}$, $r_2 = \left[(x+\mu-1)^2 + y^2\right]^{1/2}$.

Equation (1) are written in a nonuniformly rotating, barycentric, nondimensional coordinate frame where P_1 and P_2 have fixed positions $(-\mu, 0)$ and $(1-\mu, 0)$, respectively, and $\mu = m_2/(m_1 + m_2)$ is the mass parameter of the system, $\mu = 3.2262081094 \times 10^{-7}$. This coordinate frame pulsates as the P_1–P_2 distance, assumed to be the unit distance, varies according to the mutual position of the two primaries on their orbits [see Szebehely 1967 for the derivation of Eq. (1)]. The primes in Eq. (1) represent differentiation with respect to f, the true anomaly of the system. This is the independent variable, and plays the role of the time. f is zero when P_1, P_2 are at their periapse, as both primaries orbit the center of mass in similarly oriented ellipses having common eccentricity e_p. Normalizing the period of P_1, P_2 to 2π, the dependence of true anomaly on time, t, is given by

$$f(t) = f_0 + \int_{t_0}^{t} \frac{\left(1 + e_p \cos f(\tau)\right)^2}{\left(1 - e_p^2\right)^{3/2}} \, \mathrm{d}\tau, \tag{4}$$

where f_0 and t_0 are the initial true anomaly and time, respectively.

The elliptic problem possesses five equilibrium points, L_k, $k = 1, \ldots, 5$. Three of these, L_1, L_2, L_3, lie along the x-axis; the other two, L_4, L_5, lie at the vertices of two equilateral triangles with common base extending from P_1 to P_2. These points have a fixed location in the

rotating, scaled frame. However, their real distance from P_1, P_2 varies (pulsates) according to the mutual motion of the primaries. When $e_p = 0$, we obtain the planar circular restricted three-body problem.

4 Mars stable sets and ballistic capture orbits

In this section we elaborate on Step 1 in Sect. 2. The goal is to compute special ballistic capture trajectories that start far from Mars (P_2) and go to ballistic capture near Mars at a specified radial distance, r_p.

Ballistic capture trajectories can be designed by making use of stable sets associated to the algorithmic definition of weak stability boundaries (for more details the reader can refer to García and Gómez 2007; Topputo and Belbruno 2009; Romagnoli and Circi 2009; Hyeraci and Topputo 2010; Makó et al. 2010; Sousa Silva and Terra 2012a, b; Hyeraci and Topputo 2013; Makó 2014; Luo et al. 2014).

In Topputo and Belbruno (2009), the algorithmic definition of the weak stability boundary (WSB) is given in the circular restricted three-body problem, about Jupiter, where the stable sets are computed. These are computed by a definition of stability that can be easily extended to more complicated models. Stable sets are constructed by integrating initial conditions of the spacecraft about one primary and observing its motion as it cycles the primary, until the motion substantially deviates away from the primary. Special attention is made to those stable orbits that, in backwards time, deviate before one cycle. These are good for applications for minimal energy capture. Although derived by an algorithmic definition, the dynamics of stable sets can be related to those of the Lagrange points, which is a deep result (Belbruno et al. 2010; García and Gómez 2007).

More precisely, stable sets are computed by the following procedure: A grid of initial conditions is defined around one of the two primaries. These correspond to periapsis points of elliptic two-body orbits with different semi-major axis and orientation. The eccentricity is held fixed in each of the stable sets. Initial conditions are integrated forward and labeled according to the stability of the orbits they generate. In particular, an orbit is called *n-stable* if it performs n revolutions around the primary while having negative Kepler energy at each turn and without performing any revolution around the other primary. Otherwise, it is called *n-unstable*. Backward stability is introduced in Hyeraci and Topputo (2010) by studying the behavior of the orbits integrated backward in time; this defines $-m$-stability. The WSB itself occurs as the boundary of the stable regions.

In the circular restricted three-body problem, the union of all n-stable initial conditions is indicated as $\mathcal{W}_n(e)$, where e is the eccentricity used to define the initial conditions (see Topputo and Belbruno 2009). When computed in nonautonomous (i.e. time dependent) models, the initial conditions have to account for the initial time as well. If the elliptic restricted three-body problem is used, the stable sets are indicated by $\mathcal{W}_n(f_0, e)$ (The details of these definitions are summarized in "Appendix 1").

Computing stable sets involves integrating tens of thousands of orbits generated over a computational grid of points. In Hyeraci and Topputo (2010) polar coordinates are used, and therefore the grid is defined by radial, angular spacing of points. This shows up in the plots upon magnification.

It is remarked that the set of grid points is five-dimensional. The grid is fine so not to lose relevant information about the stable sets. For this reason, the computations are time intensive. The parameters (range and refinement) used in this work are: (i.) r, the radial distance to Mars, $r = R_M + h$, spacing $\Delta h = 50$ km, for $250 \leq h \leq 30{,}000$ km, and

$\Delta h = 500$ km, for $30,500 \leq h \leq 250{,}000$ km, where h is the altitude and R_M is the radius of Mars; (ii.) θ, the angular position with respect to a reference direction, $0 \leq \theta \leq 360°$, $\Delta\theta = 1°$; (iii.) e, the osculating eccentricity, $0.90 \leq e \leq 0.99$, $\Delta e = 0.01$; (iv.) f_0, the initial true anomaly of primaries, $0 \leq f_0 \leq \pi/2$, $\Delta f_0 = \pi/4$; (v.) n, the stability number, $-1 \leq n \leq 6$, $\Delta n = 1$.

The spatial part of the grid, given by $\{r, \theta\}$, requires 375,394 initial conditions which need to be numerically integrated. All numerical integrations of System (1) are done using a variable-order, multi-step Adams–Bashforth–Moulton scheme. Also, when P comes close to Mars, then a Levi–Civita regularization is used to speed up the numerical integration.

4.1 Constructing ballistic capture orbits about Mars

In Hyeraci and Topputo (2010, 2013), a method to construct ballistic capture orbits with prescribed stability number is given. This method is based on a manipulation of the stable sets. It is briefly recalled. First, let us consider the set $\mathcal{W}_{-1}(e, f_0)$: this set is made up of the initial conditions that generate -1-stable orbits; i.e., orbits that stay about the primary for at least one revolution when integrated backward. By definition, the complementary set, $\overline{\mathcal{W}}_{-1}(e, f_0)$, contains initial conditions that generate -1-unstable orbits. These are orbits that escape from the primary in backward times or, alternatively, they approach the primary in forward time. The ballistic capture orbits of practical interest are contained in the capture set

$$\mathcal{C}^n_{-1}(e, f_0) = \overline{\mathcal{W}}_{-1}(e, f_0) \cap \mathcal{W}_n(e, f_0). \tag{5}$$

The points in $\mathcal{C}^n_{-1}$ are associated to orbits that both approach the primary and perform at least n revolutions around it. This is desirable in mission analysis, as these orbits may represent good candidates to design the ballistic capture immediately upon arrival. For a well defined derivation of the capture set it is important that only those sets computed with identical values of e, f_0 are intersected. This assures the continuity along the orbits; i.e., the endpoint of the approaching (-1-unstable) orbit has to correspond to the initial point of the capture (n-stable) orbit.

The stable set $\mathcal{W}_n(e, f_0)$ is shown in Fig. 2 for different n, and given values of e, f_0. To generate these plots, N stable points are plotted. The capture set $\mathcal{C}^6_{-1}(0.99, \pi/4)$ associated to the set in Fig. 2 for $n = 6$ is shown in Fig. 3. Each point in $\mathcal{C}^6_{-1}(0.99, \pi/4)$ gives rise to an orbit that approaches Mars and performs *at least* six revolutions around it. In Fig. 4 the orbit generated by the point indicated in Fig. 3 is shown in several reference frames. If a spacecraft moves on this orbit, it will approach Mars on the dashed curve and it would remain temporarily trapped about it (solid line) without performing any maneuver. The trajectory represented by the dashed curve is a ballistic capture trajectory, or transfer, approaching the ballistic capture state that gives rise to capture orbits.

4.2 Long term behavior of the capture orbits

To design transfers that exploit the inherent dynamics in $\mathcal{C}^n_{-1}$, the long-term behavior of the capture orbits has to be analyzed. To do that, we have integrated the capture orbit in Fig. 4 backward in time for a time span equal to 50 revolutions of Mars around the Sun; i.e., 34,345 days or equivalently about 94 years. Of course, this time span is not comparable to that of a practical case, but it is anyway useful to check the long-term behavior of the capture orbits to infer features on its dynamics.

As it can be seen in Fig. 5, the capture orbit gets close to Mars (red dot). This happens approximately 80 years backward in time from the ballistic capture occurrence. Although

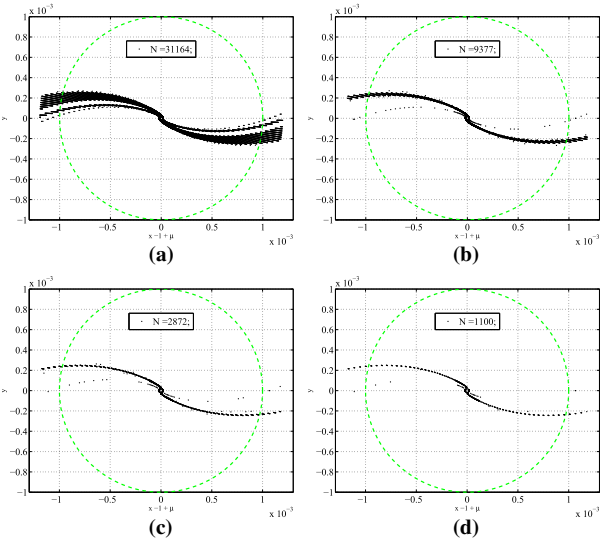

Fig. 2 Sample stable sets $\mathcal{W}_n(e,\, f_0)$ for $f_0 = \pi/4$, $e = 0.99$, $n = 1, 2, 3, 6$ ($n = 4, 5$ not reported for brevity). N is the number of stable initial conditions; the *green dashed circle* represents the Levi–Civita regularizing disc. Figures corresponding to $n = 1, 2, 3, 6$ are read from *left* to *right*, *top* to *bottom*. **a** $\mathcal{W}_1(0.99, \pi/4)$. **b** $\mathcal{W}_2(0.99, \pi/4)$. **c** $\mathcal{W}_3(0.99, \pi/4)$. **d** $\mathcal{W}_6(0.99, \pi/4)$

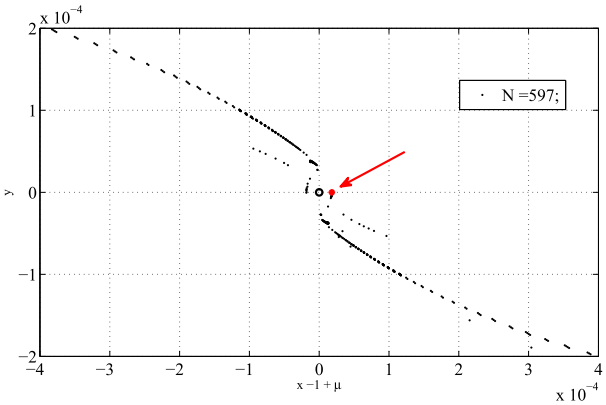

Fig. 3 Capture set $\mathcal{C}^6_{-1}(0.99, \pi/4)$

it approaches Mars, the capture orbit does not return to the stable set or the weak stability boundary about Mars, and therefore there is not a second ballistic capture within this time frame. The ballistic capture orbit does not go substantially far from the orbit of Mars within the timespan of 94 years.

4.3 Constructing ballistic capture transfers starting far from Mars

Of particular interest in this paper is to find ballistic capture transfers that start far from Mars. This is conveniently done by integrating the ballistic capture states in Fig. 3 and see where they go. We find that these trajectories, in backwards time, move far from Mars, but close to Mars orbit about the Sun. Their terminal point, $\mathbf{x}_c$, is the target for our transfers departing from the Earth. In the next section, we show how to pick this point.

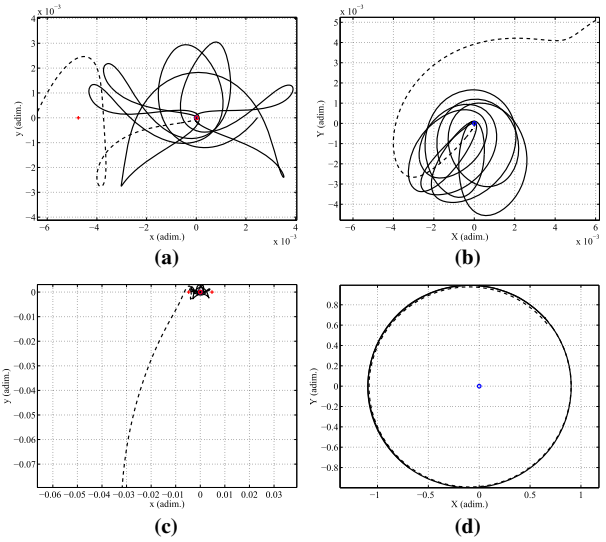

Fig. 4 Capture orbit corresponding to a point in the set $\mathcal{C}^6_{-1}(0.99, \pi/4)$ (the point indicated in Fig. 3) in rotating and inertial (Mars- and Sun-centered, respectively) coordinates. **a** Mars-centered rotating frame. **b** Mars-centered inertial frame. **c** Rotating frame, zoom out. **d** Sun-centered inertial frame

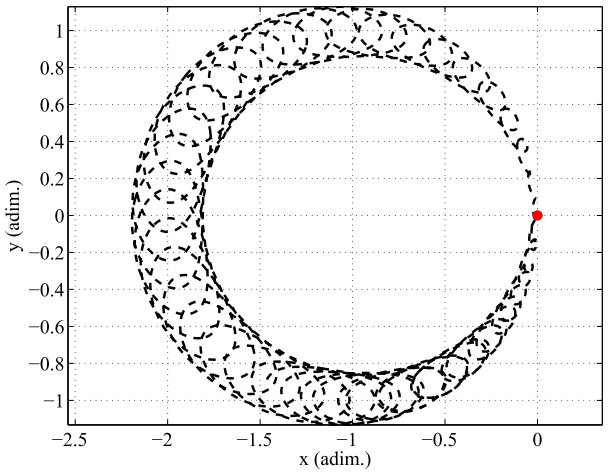

Fig. 5 Approaching portion of Fig. 4 (*dashed line*) integrated backward for a time span equal to 50 revolutions of Mars around the Sun (Sun–Mars rotating frame)

5 Interplanetary transfer from Earth to capture points far from Mars

The purpose of this section is to describe the construction of the transfer from the Earth to Mars at the ballistic capture point $\mathbf{x}_c$. This comprises Step 2 and part of Step 3 in Sect. 2. In Sect. 6 comparison to Hohmann transfers at $r = r_p$ is given, completing Step 3.

A point, $\mathbf{x}_c$, is chosen near the orbit of Mars from which to begin a ballistic capture orbit that will go to ballistic capture to Mars at a periapsis distance r_p. We choose it in an arbitrary fashion, but to be beyond the SOI of Mars, so that the gravitational force of Mars there is negligibly small. This point is obtained by integrating a point in $\mathcal{C}^n_{-1}$ in backwards time, so that it moves sufficiently far from Mars. An example of this is seen in Fig. 4 for the particular capture trajectory shown in Sect. 4. In that case we choose $\mathbf{x}_c$ about 1 million km from Mars (see Fig. 6b). When we consider different capture trajectories near a given case such as the one shown in Fig. 6b, with different properties, such as different values of r_p, then as the

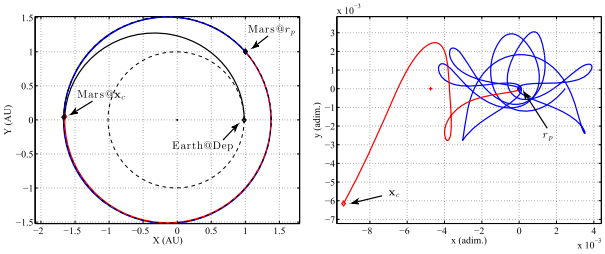

Fig. 6 A sample solution (Case 1) constructed by using the orbit in Fig. 4. *Left*: Sun-centered frame (the *black orbit* is the orbit that targets $\mathbf{x}_c$ departing from the Earth; the *red orbit* is the capture orbit; the *blue orbit* is the post-capture orbit). *Right*: the capture orbit (*red*) and the post-capture orbit (*blue*) in the rotating Mars-centered frame. **a** Inertial frame. **b** Rotating frame

trajectory is integrated backwards, different values of $\mathbf{x}_c$ are obtained that lie relatively close to each other. This variation of $\mathbf{x}_c$ occurs in the general optimization algorithm described in Sect. 5.2.

5.1 Dynamics of capture and complete transfer from Earth to Mars ballistic capture

The interplanetary transfer together with the ballistic capture orbit comprise the whole transfer from the Earth to Mars. An example of this is given in Fig. 6 (we refer to as Case 1). When P arrives at $\mathbf{x}_c$ it is trailing Mars by approximately 1 million km. However, P is moving slightly faster than Mars as P leaves $\mathbf{x}_c$ on the ballistic capture transfer. Approximately a year later, P catches up to Mars and slightly overtakes it, passing near to L_1. P is then pulled in towards Mars for ballistic capture to r_p, and then into a set of capture orbits with at least six orbits about Mars. The capture dynamics near Mars is illustrated in Fig. 6b. This approximate 1 year transit time of the ballistic capture transfer could be significantly reduced if at $\mathbf{x}_c$ a tiny Δv were applied so that there is a faster rate of decrease of distance between P and Mars. This analysis is out of the scope of this paper and left for future study.

Another example of a complete ballistic capture transfer from the Earth is shown in Fig. 7 (we refer to as Case 2). The dynamics of capture is analogous to the previous case, where P arrives at $\mathbf{x}_c$ trailing Mars and slowly catches up for ballistic capture at r_p. In this case, x_c is approximately 23 million km from Mars.

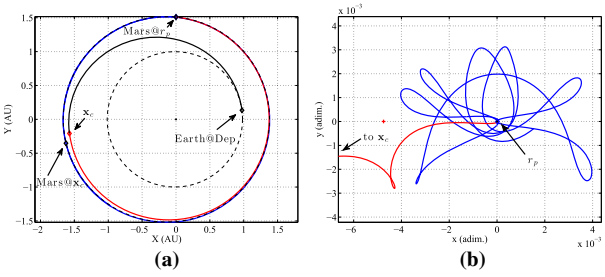

Fig. 7 A sample solution (Case 2) obtained by targeting a point in $\mathcal{C}^6_{-1}(0.99, \pi/2)$. This solution is interesting due to the fact the target point $\mathbf{x}_c$ is 23×10^6 km from Mars. Also, it takes approximately the same time to reach r_p as the case in Fig. 6. *Left*: Sun-centered inertial frame. *Right*: rotating Mars-centered frame. **a** Inertial frame. **b** Rotating frame

The post-capture orbits about Mars after P arrives at r_p are different for Case 1 and Case 2. They look similar in appearance but occur for different locations in the capture set, $C^6_{-1}(0.99, f_0)$, where $f_0 = \pi/4, \pi/2$, respectively.

5.2 Optimization of transfers from Earth to Mars ballistic capture

The transfers from Earth to ballistic capture at Mars are sought under the following assumptions: 1) The equations describing the ballistic capture dynamics are those of the planar, elliptic restricted three-body problem; 2) The whole transfer is planar, that is, the Earth and Mars are assumed to revolve in coplanar orbits; 3) A first maneuver, ΔV_1, is performed to leave the Earth. This is computed by assuming the spacecraft as being already in heliocentric orbit at the Earth's SOI; 4) A second maneuver, ΔV_c, is performed to inject the spacecraft into the ballistic capture orbit; 5) In between the two maneuvers, the spacecraft moves in the heliocentric space far from both the Earth and Mars, and therefore the dynamics is that of the two-body problem (Topputo et al. 2005).

The *parameters* of the optimization (to be picked and held fixed) are:

- The capture set. The stable sets computed keep fixed eccentricity and initial true anomaly. Moreover, when the capture sets are defined from the stable sets, the stability number has to be decided. Therefore, selecting a pre-computed capture set (5) means fixing 1) the osculating eccentricity e of the first post-capture orbit; 2) the initial true anomaly f_0 of Mars orbit; 3) the stability number n, or the minimum number of natural revolutions around Mars.
- The initial capture orbit within the set. For example, this is equivalent to specifying the radial and angular position for each of the black dots in Fig. 3, and choosing one of these. In practice, this selection yields a natural number, $j \in \{1, 2, \ldots, N\}$.

The *variables* of the optimization problem are:

- The true anomaly f at the end of the backward integration, $f < f_0$. This is needed to define $\mathbf{x}_c$ by starting from r_p and performing a backward integration, $\mathbf{x}_c(f) = \varphi(\mathbf{x}_p(r_p), f_0; f)$, where φ is the flow of system (1) and $\mathbf{x}_p(r_p)$ is the periapsis state [see Hyeraci and Topputo (2010) for the expression of $\mathbf{x}_p(r_p)$].
- The time of flight T from the Earth to the target point $\mathbf{x}_c$. This is needed to solve the Lambert problem once the position of the Earth is known.
- A phase angle θ to specify the position of the Earth on its orbit.

The *objective function* is the cost of the second maneuver, ΔV_c. It is assumed that the first maneuver, ΔV_1, can be always achieved. Moreover, it is expected that the cost for ΔV_1 is equivalent to that of a standard Hohmann transfer as the target point is from an angular perspective, not too far from Mars. The optimization algorithm adjusts f, and hence the location of $\mathbf{x}_c$, as well as T, θ to minimize ΔV_c.

6 Comparison of ballistic capture transfer to Hohmann

The parameters for the reference Hohmann transfers from Earth SOI to Mars SOI are listed in Table 5 in "Appendix 2"; these figures correspond to geometries where four different bitangential transfers are possible. The hyperbolic excess velocity at Mars SOI for these bitangential transfers are listed in Table 1. These will be taken as reference solutions to compare the ballistic capture transfers derived in this paper. These four reference solutions

Table 1 Hyperbolic excess velocities at Mars for the four bitangential transfers in "Appendix 2"

Case	V_∞ (km/s)
H1	3.388
H2	2.090
H3	3.163
H4	1.881

represent a lower bound for all possible patched-conics transfers: when the transfer orbit is not tangential to Mars orbit, the hyperbolic excess velocity increases.

When approaching Mars in hyperbolic state with excess velocity V_∞ at Mars SOI, the cost to inject into an elliptic orbit with fixed eccentricity e and periapsis radius r_p is straight forward to compute as,

$$\Delta V_2 = \sqrt{V_\infty^2 + \frac{2\mu_M}{r_p}} - \sqrt{\frac{\mu_M(1+e)}{r_p}} \tag{6}$$

where μ_M is the gravitational parameters of Mars (see Table 4, "Appendix 2"). This formula is used to compute the ΔV_2 for different values of r_p.

It is important to note that a main goal of this paper is to study the performance of the ballistic capture transfers from the Earth to Mars from the perspective of the capture Δv as compared to Hohmann transfers, when going to specific periapsis radii, r_p. This is done irrespective of ΔV_1. However, in Cases 1 and 2, $\mathbf{x}_c$ is 1 and 23 million km from Mars, respectively, and because of this, the value of ΔV_1 for both Hohmann and ballistic capture transfers are approximately the same. Thus, in these cases, studying the capture Δv performance is equivalent to the total Δv performance.

An assessment of the ballistic capture transfers whose $\mathbf{x}_c$ states are originated by the sets $\mathcal{C}^6_{-1}(e, f_0)$, with $e = 0.99$ and $f_0 = 0, \pi/4, \pi/2$, has been made. f_0 is chosen in the first quadrant, consistent with the arguments in Hyeraci and Topputo (2013). The results are summarized in Fig. 8. In these figures, the red dots represent the ΔV_c cost of the ballistic capture solutions, whereas the blue curves are the functions $\Delta V_2(r_p)$ computed from (6) associated to the four bitangential Hohmann transfers in Table 5 (see the labels in the rightmost part of the figures). From inspection of Fig. 8 it can be seen that the ballistic capture transfers are more expensive than all of the Hohmann transfers for low altitudes. Nevertheless, when r_p increases, the ballistic capture transfers perform better than H1 and H3. This occurs at periapsis radii $r_p^{(1)}$ and $r_p^{(2)}$, respectively, whose values are reported in Table 2 along with the values for which $\Delta V_c \simeq \Delta V_2$. For periapsis radii above $r_p^{(1)}$ or $r_p^{(2)}$, the savings increase for increasing r_p. In the cases of H2, H4, the ballistic capture transfers do not perform as well as the Hohmann transfers for any value of r_p.

A number of observations arise from the assessment performed. These are briefly given below.

- The cost for the ballistic capture transfers is approximately constant regardless of the periapsis radius r_p. This is a big departure from Hohmann transfers where the cost increases for increasing r_p.
- The red dots in Fig. 8 are organized into two different sets that correspond to the two branches of the capture sets, see Fig. 3.

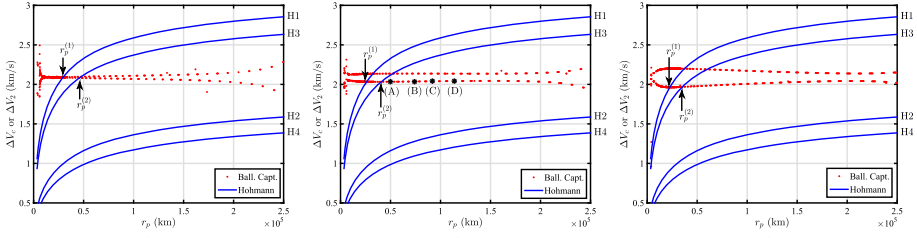

Fig. 8 Comparison of Hohmann bitangential transfers and ballistic capture transfers originated by the capture sets $\mathcal{C}(e,\, f_0)$, $e = 0.99$, $f_0 = 0, \pi/4, \pi/2$. **a** $f_0 = 0$. **b** $f_0 = \pi/4$. **c** $f_0 = \pi/2$

Table 2 Periapsis radii for which the ballistic capture transfers become more convenient than the Hohmann transfers for different f_0

f_0	$r_P^{(1)}$ (km)	$r_P^{(2)}$ (km)	ΔV_c (km/s)
0	29×10^3	46×10^3	2.09
$\pi/4$	26×10^3	40×10^3	2.03
$\pi/2$	22×10^3	34×10^3	1.96

Table 3 Comparison between ballistic capture transfers and Hohmann transfers for the points in Fig. 8b

Point	r_P (km)	ΔV_c (km)	ΔV_2 (km/s)	S (%)	$\Delta t_{c\to p}$ (days)
(A)	49,896	2.033	2.116	−4.0	434
(B)	73,896	2.036	2.267	−11.3	433
(C)	91,897	2.039	2.344	−14.9	432
(D)	113,897	2.041	2.414	−18.2	431

The saving, S, is computed as $S = (\Delta V_c - \Delta V_2)/\Delta V_c$, where the ΔV_2 associated to the H3 case is considered. S is a measure of the efficiency of the ballistic capture transfers. $\Delta t_{c\to p}$ is the time-of-flight needed to go from $\mathbf{x}_c$ to r_p

– The set of red dots, as a function of r_p is seen to have a series of gaps. This is due to the structure of the stable and unstable sets associated to the algorithmic definition (see "Appendix 1"). As is described in Topputo and Belbruno (2009), Belbruno et al. (2010), the stable and unstable sets alternate on each radial line emanating from the secondary body (Mars in this case), giving a Cantor-like structure.

The results from Fig. 8b are summarized in Table 3. From this table it can be seen that the time for the spacecraft to go from $\mathbf{x}_c$ to r_p is on the order of a year.

It is remarked that in the cases considered for $e = .99$, as the capture orbits cycle about Mars with high periapsis values, they will have apoapsis values beyond the SOI of Mars. Since the SOI is purely a geometric definition associated to two-body motion, and not based on actual three-body dynamics, these orbits are well defined outside of the SOI. The fact they exist in the elliptic restricted problem demonstrates this.

In summary, we have the following,

Result A —The ballistic capture transfers use less ΔV for the capture process than a Hohmann transfer for altitudes above $r_p^{(1)}, r_p^{(2)}$ in the cases for H1, H3 in the examples given, where

$$\Delta V_c < \Delta V_2. \tag{7}$$

6.1 Low values of e

The osculating value of e at r_p considered in our analysis is $e = .99$. It is of interest to see what happens when e is reduced to lower values. The case of $e = .90$ is considered. This is a capture state where the capture should be more stable. This means that the post capture trajectory can generally move about Mars with more orbits before becoming unstable and escaping Mars. Therefore, it is expected that the structure of the capture set for $e = .99$ shown in Fig. 3 will change significantly since the possibility of ballistic capture at lower values of e is less likely. This is seen in Fig. 9a. The points are more clustered to distances

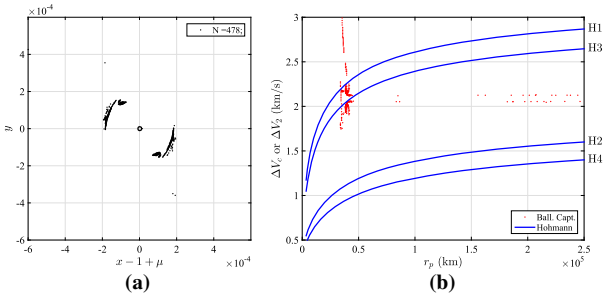

Fig. 9 The capture set and the cost profile associated to $e = 0.90$. **a** $\mathcal{C}^6_{-1}(0.90, \pi/4)$. **b** Solutions cost

close to Mars. The available capture points are much more sparse as the capture radius r_p increases. This is reflected in Fig. 9b. An interesting feature is seen in Fig. 9b, where many capture possibilities exist near the altitude of approximately 40,000 km. It is seen that there exist many points where $\Delta V_c < \Delta V_2$.

6.2 Low values of r_p, launch period flexibility

The fact that one can have $\mathbf{x}_c$ far from Mars has an implication on the launch period from the Earth to get to Mars. For the case of a Hohmann transfer, there is a small launch period of a few days that must be satisfied when Mars and the Earth line up. If this is missed for any reason, a large penalty in cost may occur since launch may not be possible. This problem would be alleviated if the launch period could be extended. By targeting to $\mathbf{x}_c$ rather than to Mars, it is not necessary to wait every 2 years, but rather, depending on how far $\mathbf{x}_c$ is separated from Mars, the time of launch could be extended significantly.

This launch period flexibility has another implication. As determined in this paper, the Hohmann transfer is cases H1, H3 uses more capture Δv than a ballistic capture transfer when $r_p > r_p^{(1)}, r_p^{(2)}$. Since the capture Δv used by the ballistic capture transfer and the Hohmann tansfer is the same when $r_p = r_p^{(1)}, r_p^{(2)}$, then the penalty, or excess, Δv that a ballistic capture uses relative to a Hohmann transfer when transferring to a lower altitude can be estimated by just calculating the Δv's to go from a ballistic capture state at $r_p = r_p^{(1)}, r_p^{(2)}$ to a desired altitude lower than these, say to a periapsis altitude of 100 km, where $r_p = r_p^* = 100 + R_M$.

For example, let us consider the case where we transfer from $r_p = 40,000$ km to r_p^*, with $e = .99$. (In this case, the orientation of the larger ellipse of periapsis altitude r_p is 180° different from the smaller ellipse of periapsis radius r_p^*.) To make this transfer, it is calculated that the spacecraft must change velocity by .196 km/s at r_p and by .192 km/s at r_p*. This yields a total value of .380 km/s. This number may be small enough to justify a ballistic capture transfer instead of a Hohmann transfer if it was decided that the flexibility of launch period was sufficiently important.

7 Applications and future work

The capture Δv savings offered by the ballistic capture transfer from the Earth to Mars is substantial when transferring to higher altitudes under our assumptions. This may translate into considerable mass fraction savings for a spacecraft arriving at Mars, thereby allowing more payload to be placed into orbit or on the surface of Mars, over traditional transfers to Mars, which would be something interesting to study. Although the Hohmann transfer

provides lower capture Δv performance in certain situations, in other cases it doesn't, and in these the ballistic capture transfer offers an alternative approach. It is remarked that we are considering reference Hohmann transfers that perform a single capture maneuver at r_p. Multi-burn capture strategies exploiting the Oberth effect can be more efficient, and are not considered in this paper. This is a topic for further study.

It isn't the capture performance that is the only interesting feature. A very interesting feature mentioned in Sect. 6.2 is that by targeting to points near Mars orbit to start a ballistic capture transfer, the target space opens considerably from that of a Hohmann transfer which must transfer directly to Mars. By transferring from the Earth to points far from Mars, the time of launch from the Earth opens up and is much more flexible. This flexibility of launch period offers a new possibility for Mars missions. For example, if a launch vehicle is not able to be launched within the required window, a latter time can be chosen without canceling the mission. Also the methodology of first arriving far from Mars offers a new way to send spacecraft to Mars that may be beneficial from an operational point of view. This launch flexibility and new operational framework offer new topics to study in more depth.

In case low altitude orbits are desired, a number of injection opportunities arise during the multiple periapsis passages on the cycling capture ellipses to transfer to a lower altitude, as described in Sect. 6.2. This is safer from an operational point of view to achieve low orbit, although only slightly more Δv is used. When this is coupled to the flexibility of the launch period, it may be beneficial to pay the extra ΔV.

Another advantage of using the ballistic capture option is the benign nature of the capture process as compared to the Hohmann transfer. The capture Δv is done far from Mars and can be done in a gradual and safe manner. Also, when the spacecraft arrives to Mars periapsis to go into orbit on the cycling ellipses, no Δv is required. By comparison, the capture process for a Hohmann transfer needs to be done very quickly at the point of closest approach, or the spacecraft is lost. An example of this was the Mars Observer mission.

Although the time of flight is longer as compared with a Hohmann transfer, this is only due to the choice of $\mathbf{x}_c$. By performing a minor adjustment to ΔV_c, the time of flight to Mars should be able to be reduced, which is an interesting topic to study for future work. Moreover, it would be of interest to understand how this methodology could be applied for transfers to other inner planets or to the moons of the outer planets

This new class of transfers to Mars offers alternative mission design possibilities for Mars missions.

Acknowledgments We would like to thank the Boeing Space Exploration Division for sponsoring this work, and, in particular, we would like to thank Kevin Post and Michael Raftery. We would also like to thank Cesar Ocampo of NASA JSC for helpful comments.

Appendix 1: Summary of precise definitions of stable sets and weak stability boundary

Trajectories of P satisfying the following conditions are studied (see García and Gómez 2007; Topputo and Belbruno 2009; Hyeraci and Topputo 2010).

(i) The initial position of P is on a radial segment $l(\theta)$ departing from P_2 and making an angle θ with the P_1–P_2 line, relative to the rotating system. The trajectory is assumed to start at the periapsis of an osculating ellipse around P_2, whose semi-major axis lies on $l(\theta)$ and whose eccentricity e is held fixed along $l(\theta)$.
(ii) In the P_2-centered inertial frame, the initial velocity of the trajectory is perpendicular to $l(\theta)$, and the Kepler energy, H_2, of P relative to P_2 is negative; i.e., $H_2 < 0$ (ellipse

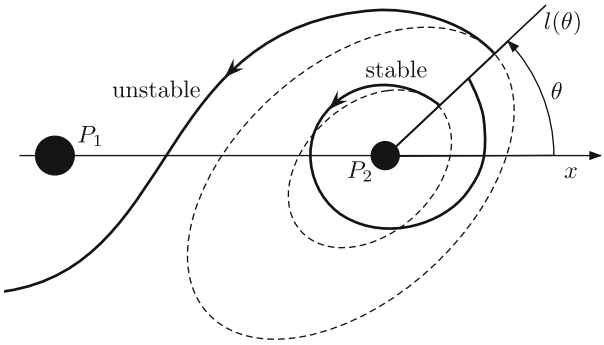

Fig. 10 Stable and unstable motions

periapsis condition). The motion, for fixed values of e, f_0, θ depends on the initial distance r only.

(iii) The motion is said to be n-stable if the infinitesimal mass P leaves $l(\theta)$, makes n complete revolutions about P_2, $n \geq 1$, and returns to $l(\theta)$ on a point with negative Kepler energy with respect to P_2, *without* making a complete revolution around P_1 along this trajectory. The motion is otherwise said to be n-unstable (see Fig. 10).

The set of n-stable points on $l(\theta)$ is a countable union of open intervals

$$\mathcal{W}_n(\theta, e, f_0) = \bigcup_{k \geq 1} \left(r^*_{2k-1}, r^*_{2k}\right), \tag{8}$$

with $r^*_1 = 0$. The points of type r^* (the endpoints of the intervals above, except for r^*_1) are n-unstable. Thus, for fixed pairs (e, f_0), the collection of n-stable points is

$$\mathcal{W}_n(e, f_0) = \bigcup_{\theta \in [0, 2\pi]} \mathcal{W}_n(\theta, e, f_0). \tag{9}$$

The weak stability boundary of order n, $\partial\mathcal{W}_n$, is the locus of all points $r^*(\theta, e, f_0)$ along the radial segment $l(\theta)$ for which there is a change of stability of the trajectory; i.e., $r^*(\theta, e, f_0)$ is one of the endpoints of an interval (r^*_{2k-1}, r^*_{2k}) characterized by the fact that, for all $r \in (r^*_{2k-1}, r^*_{2k})$, the motion is n-stable, and there exist $\tilde{r} \notin (r^*_{2k-1}, r^*_{2k})$, arbitrarily close to either r^*_{2k-1} or r^*_{2k} for which the motion is n-unstable. Thus,

$$\partial\mathcal{W}_n(e, f_0) = \{r^*(\theta, e, f_0) \,|\, \theta \in [0, 2\pi]\}.$$

Appendix 2: Computation of reference Hohmann transfers

The physical constants used in this work are listed in Table 4. As both the Earth and Mars are assumed as moving on elliptical orbits, there are four cases in which a bitangential transfer is possible, depending on their relative geometry. These are reported in Table 5, where '@P' and '@A' mean 'at perihelium' and 'at aphelium', respectively. In Table 5, ΔV_1 is the maneuver needed to leave the Earth orbit, whereas $\Delta V_{2,\infty}$ is the maneuver needed to acquire the orbit of Mars; these two impulses are calculated by considering the spacecraft already in heliocentric orbit, and therefore ΔV_1, $\Delta V_{2,\infty}$ are equivalent to the escape, incoming hyperbolic velocities, respectively. ΔV and Δt are the total cost and flight time, respectively. The use of the notation, $\Delta V_{2,\infty}$ is to distinguish from the use of ΔV_2 used in Sect. 6 for the actual maneuver cost at r_p.

Table 4 Physical constants used in this work

Symbol	Value	Units	Meaning
μ_S	1.32712×10^{11}	km^3/s^2	Gravitational parameter of the Sun
AU	149,597,870.66	km	Astronomical unit
μ_E	3.98600×10^5	km^3/s^2	Gravitational parameter of the Earth
a_E	1.000000230	AU	Earth orbit semimajor axis
e_E	0.016751040	–	Earth orbit eccentricity
μ_M	4.28280×10^4	km^3/s^2	Gravitational parameter of Mars
a_E	1.523688399	AU	Mars orbit semimajor axis
e_E	0.093418671	–	Mars orbit eccentricity

Table 5 Bitangential transfers and Hohmann transfer

Case	Earth	Mars	ΔV_1 (km/s)	$\Delta V_{2,\infty}$ (km/s)	ΔV (km/s)	Δt (days)
H1	@P	@P	2.179	3.388	5.568	234
H2	@P	@A	3.398	2.090	5.488	278
H3	@A	@P	2.414	3.163	5.577	239
H4	@A	@A	3.629	1.881	5.510	283

From the figures in Table 5 it can be inferred that although the total cost presents minor variations among the four cases, the costs for the two maneuvers change considerably. That is, by arbitrary picking one of the four bitangential solutions as reference we can have different outcomes on the performance of the ballistic capture orbits devised. Because there is a substantial variation, an averaging does not yield useful results, and therefore, each case is considered.

References

Belbruno, E.: Capture Dynamics and Chaotic Motions in Celestial Mechanics: With Applications to the Construction of Low Energy Transfers. Princeton University Press, Princeton (2004)

Belbruno, E., Miller, J.: Sun-perturbed Earth-to-Moon transfers with ballistic capture. J. Guid. Control Dyn. **16**, 770–775 (1993)

Belbruno, E., Gidea, M., Topputo, F.: Weak stability boundary and invariant manifolds. SIAM J. Appl. Dyn. Syst. **9**(3), 1061–1089 (2010). doi:10.1137/090780638

Belbruno, E., Gidea, M., Topputo, F.: Geometry of weak stability boundaries. Qual. Theory Dyn. Syst. **12**(1), 53–66 (2013). doi:10.1007/s12346-012-0069-x

Belbruno, E., Topputo, F., Gidea, M.: Resonance transition associated to weak capture in the restricted three-body problem. Adv. Space Res. **42**(8), 18–39 (2008). doi:10.1016/j.asr.2008.01.018

Castillo, A., Belló-Mora, M., Gonzalez, J.A., Janint, G., Graziani, F., Teofilatto, P., Circi, C.: Use of weak stability boundary trajectories for planetary capture. In: Paper IAF-03-A.P.31, Proceedings of the International Astronautical Conference (2003)

Chung, M.J., Hatch, S.J., Kangas, J.A., Long, S.M., Roncoli, R.B., Sweetser, T.H.: Trans-lunar cruise trajectory design of GRAIL (Gravity Recovery and Interior Laboratory) Mission. In: Paper AIAA 2010–8384, AIAA Guidance, Navigation, and Control Conference, Toronto, Ontario, Canada, 2–5 Aug (2010)

García, F., Gómez, G.: A note on weak stability boundaries. Celest. Mech. Dyn. Astron. **97**, 87–100 (2007). doi:10.1007/s10569-006-9053-6

Hyeraci, N., Topputo, F.: Method to design ballistic capture in the elliptic restricted three-body problem. J. Guid. Control Dyn. **33**(6), 1814–1823 (2010). doi:10.2514/1.49263

Hyeraci, N., Topputo, F.: The role of true anomaly in ballistic capture. Celest. Mech. Dyn. Astron. **116**(2), 175–193 (2013). doi:10.1007/s10569-013-9481-z

Lo, M.W., Ross, S.D.: Low energy interplanetary transfers using the invarian manifolds of L_1, L_2, and halo orbits. In: Paper AAS 98–136, Proceedings of the AAS/AIAA Space Flight Mechanics Meeting (1998)

Luo, Z.F., Topputo, F., Bernelli-Zazzera, F., Tang, G.J.: Constructing ballistic capture orbits in the real solar system model. Celest. Mech. Dyn. Astron. **120**(4), 433–452 (2014). doi:10.1007/s10569-014-9580-5

Makó, Z.: Connection between hill stability and weak stability in the elliptic restricted three-body problem. Celest. Mech. Dyn. Astron. **120**(3), 233–248 (2014). doi:10.1007/s10569-014-9577-0

Makó, Z., Szenkovits, F., Salamon, J., Oláh-Gál, R.: Stable and unstable orbits around Mercury. Celest. Mech. Dyn. Astron. **108**(4), 357–370 (2010). doi:10.1007/s10569-010-9309-z

Mingotti, G., Topputo, F., Bernelli-Zazzera, F.: Earth–Mars transfers with ballistic escape and low-thrust capture. Celest. Mech. Dyn. Astron. **110**(2), 169–188 (2011). doi:10.1007/s10569-011-9343-5

Romagnoli, D., Circi, C.: Earth–Moon weak stability boundaries in the restricted three and four body problem. Celest. Mech. Dyn. Astron. **103**(1), 79–103 (2009). doi:10.1007/s10569-008-9169-y

Schoenmaekers, J., Horas, D., Pulido, J.A.: SMART-1: with solar electric propulsion to the Moon. In: Proceeding of the 16th International Symposium on Space Flight Dynamics (2001)

Sousa Silva, P., Terra, M.: Applicability and dynamical characterization of the associated sets of the algorithmic weak stability boundary in the lunar sphere of influence. Celest. Mech. Dyn. Astron. **113**(2), 141–168 (2012a). doi:10.1007/s10569-012-9409-z

Sousa Silva, P., Terra, M.: Diversity and validity of stable–unstable transitions in the algorithmic weak stability boundary. Celest. Mech. Dyn. Astron. **113**(4), 453–478 (2012b). doi:10.1007/s10569-012-9418-y

Szebehely, V.: Theory of Orbits: The Restricted Problem of Three Bodies. Academic Press Inc, London (1967)

Topputo, F.: On optimal two-impulse Earth–Moon transfers in a four-body model. Celest. Mech. Dyn. Astron. **117**(3), 279–313 (2013). doi:10.1007/s10569-013-9513-8

Topputo, F., Belbruno, E.: Computation of weak stability boundaries: Sun–Jupiter system. Celest. Mech. Dyn. Astron. **105**(1–3), 3–17 (2009). doi:10.1007/s10569-009-9222-5

Topputo, F., Belbruno, E., Gidea, M.: Resonant motion, ballistic escape, and their applications in astrodynamics. Adv. Space Res. **42**(8), 6–17 (2008). doi:10.1016/j.asr.2008.01.017

Topputo, F., Vasile, M., Bernelli-Zazzera, F.: Low energy interplanetary transfers exploiting invariant manifolds of the restricted three-body problem. J. Astron. Sci. **53**(4), 353–372 (2005)